Tuning sound with soft dielectrics

IOP Publishing Smart Materials and Structures
Smart Mater. Struct. 26 (2017) 045028 (10pp) https://doi.org/10.1088/1361-665X/aa6387

Tuning sound with soft dielectrics

Eliana Bortot and Gal Shmuel

Faculty of Mechanical Engineering, Technion-Israel Institute of Technology, Haifa 32000, Israel

E-mail: meshmuel@tx.technion.ac.il

Received 24 November 2016, revised 30 January 2017
Accepted for publication 28 February 2017
Published 14 March 2017

Abstract

Soft dielectric tubes undergo large deformations when subjected to radial voltage. Using the theory of nonlinear electroelasticity, we investigate how voltage-controlled deformations of these tubes in an array alter acoustic wave propagation through it. We show that the propagation is annihilated across a certain audible frequency range, referred to as a sonic *band gap*. We carry out a numerical study, to find that the band gap depends nonlinearly on the voltage, owing to geometrical and material nonlinearities. By analyzing different mechanical constraints, we demonstrate that snap-through instabilities resulting from these nonlinearities can be harnessed to achieve sharp transitions in the gap width. Our conclusions hint at a new strategy to adaptively filter sound using a simple control parameter—an applied voltage.

Keywords: dielectric elastomer, tunable phononic crystal, wave propagation, nonlinear elasticity, snap-through instability, acoustics, sonic band gap

(Some figures may appear in colour only in the online journal)

1. Introduction

A periodic repetition of solids in air obstructs the propagation of sound across certain frequencies—acoustic waves undergo multiple scattering when encountering the solid phases, and subsequent Bragg interference prohibits the propagation of particular wavelengths (Gorishnyy *et al* 2005). These composites are referred to as *phononic crystals*, and such ranges of obstructed frequencies are referred to as Bragg *band gaps* (Kushwaha *et al* 1993, Sigalas and Economou 1996a, Hussein *et al* 2014). It follows that phononic crystals can be exploited to reduce noise and create acoustic isolators (Sánchez-Pérez *et al* 1998, Vasseur *et al* 2002, 2008, Babaee *et al* 2016), or conversely guide sound (Picó *et al* 2013).

Phononic crystals comprising linear elastic solids, having a fixed band structure upon fabrication, were initially investigated (Sigalas and Economou 1992, Kushwaha *et al* 1998, Vasseur *et al* 2002). The development of *smart* materials, able to sustain large strains and change their properties under external stimuli, paved a new way to achieve *tunable* gaps (Goffaux and Vigneron 2001, Barnwell *et al* 2017). The merit of composites made of such constituents is clear—they can accommodate varying applicational demands. Among the types explored are mechanically tuned elastomers (Wang and Bertoldi 2012, Babaee *et al* 2016), magnetostrictive materials (Robillard *et al* 2009), and *soft dielectrics* (Yang and Chen 2008).

Soft dielectrics undergo finite deformations and their electromechanical response changes in the presence of electric field (Pelrine *et al* 2000, Liu *et al* 2009, Brochu and Pei 2010, Schlaak *et al* 2016). Owing to these characteristics, together with their fast response, light weight and low cost, dielectric elastomers were suggested as the building blocks in structures for wave manipulation (Gei *et al* 2011, Getz *et al* 2016, Jia *et al* 2016, Shmuel and Pernas-Salomón 2016, Wu *et al* 2016, Yu *et al* 2016). In this work, we demonstrate the tunability of acoustic gaps across audible frequencies, using an array of deformable dielectric tubes. To this end, we exploit voltage-induced changes in the volume enclosed by the outer boundary of the tubes, as this filling fraction dominates the gap width (Kushwaha 1997, Sánchez-Pérez *et al* 1998). We find that the gap depends nonlinearly on the voltage, owing to geometrical and material nonlinearities. We also find that by harnessing *snap-through* instabilities resulting from these nonlinearities, sharp transitions in the gap width are accessible. While instabilities were conventionally considered as failure states, a series of recent works has shown that they can be exploited for different functionalities in discrete (Frazier and Kochmann 2017), soft (Shim *et al* 2013, Overvelde and Kloek 2015, Raney *et al* 2016), and dielectric systems (Keplinger *et al* 2012, Li *et al* 2013). Our

findings above were rendered evident since we used a proper nonlinear electroelastic theory (Dorfmann and Ogden 2005, Suo *et al* 2008, Castañeda and Siboni 2012, Lopez-Pamies 2014). This framework accounts for the nonlinear coupling between electrostatics and large deformation elasticity, and nonlinearities in the constitutive behavior of elastomers. The aforementioned results were veiled from Yang and Chen (2008), who conceived a similar system, due to their use of inadequate small-strain linear elasticity theory.

The paper is sectioned as follows. A concise summary on nonlinear electroelasticity is given section 2. Based on this theory, section 3 details first the response of a deformable dielectric tube to a radial voltage difference; subsequently, we provide the equations governing acoustic waves in an array of these actuated tubes. By way of a numerical study, we explore in section 4 how the mechanical constraints and the applied voltage tune acoustic band gaps. Concluding remarks complete the paper in section 5.

2. Finite electroelasticity

The motion of a particle in a deformable body is described by the vector field $\boldsymbol{\chi}$, mapping it from its initial position $\mathbf{X}$ in reference configuration Ω_0 to its current configuration Ω at time t, according to $\mathbf{x} = \boldsymbol{\chi}(\mathbf{X}, t)$. The corresponding velocity and acceleration fields are $\mathbf{v} = \boldsymbol{\chi}_{,t}$ and $\mathbf{a} = \boldsymbol{\chi}_{,tt}$, respectively. The deformation gradient $\mathbf{F} = \nabla_{\mathbf{X}}\boldsymbol{\chi}$ maps lines elements in the vicinity of $\mathbf{X}$, where $\nabla_{\mathbf{X}}(\bullet)$ denotes differentiation with respect to the reference coordinates. Its determinant $J = \det \mathbf{F}$ is the ratio between an infinitesimal volume element in the deformed configuration, $\mathrm{d}v$, and its counterpart in the reference configuration, $\mathrm{d}V$. Accordingly, the condition $J = 1$ is implied for deformations of incompressible bodies. The left Cauchy–Green tensor $\mathbf{b} = \mathbf{F}\mathbf{F}^{\mathrm{T}}$ provides a measure of the resultant strain.

The electrical field and the electric displacement field in a dielectric body, denoted respectively by $\mathbf{e}$ and $\mathbf{d}$, are governed by Maxwell equations. In the quasi-electrostatic approximation for dielectrics, these read

$$\nabla \cdot \mathbf{d} = 0, \quad \nabla \times \mathbf{e} = \mathbf{0}. \tag{1}$$

The second of equation (1) implies that $\mathbf{e}$ can be derived from a scalar field φ, such that $\mathbf{e} = -\nabla\varphi(\mathbf{x})$.

In absence of mechanical body forces, the equations of motion read

$$\nabla \cdot \boldsymbol{\sigma} = \rho\mathbf{a}, \tag{2}$$

where ρ is the mass density of the material in the current configuration, and $\boldsymbol{\sigma}$ is the *total* stress tensor, which accounts for both mechanical and electrical forces. The balance of the angular momentum enforces the symmetry of the total stress.

Across the outer boundary of the body, the following jump conditions hold

$$\begin{aligned}(\boldsymbol{\sigma} - \boldsymbol{\sigma}^\star)\mathbf{n} = \mathbf{t}_m, \quad (\mathbf{e} - \mathbf{e}^\star) \times \mathbf{n} = \mathbf{0},\\ (\mathbf{d} - \mathbf{d}^\star) \cdot \mathbf{n} = -\omega_e.\end{aligned} \tag{3}$$

Here, $\mathbf{n}$ is the outward unit normal vector of an element in the deformed configuration, $\mathbf{t}_m$ is a prescribed mechanical traction, ω_e is the surface charge density, $\mathbf{d}^\star$ is the outer electric displacement field, and $\boldsymbol{\sigma}^\star$ is the Maxwell stress outside the body. In terms of the outer electric field $\mathbf{e}^\star$, Maxwell stress reads

$$\boldsymbol{\sigma}^\star = \epsilon_0\left[\mathbf{e}^\star \otimes \mathbf{e}^\star - \frac{1}{2}(\mathbf{e}^\star \cdot \mathbf{e}^\star)\mathbf{I}\right], \tag{4}$$

where $\mathbf{I}$ is the identity tensor and ϵ_0 is the vacuum permittivity.

When large deformations take place, it is convenient to employ a Lagrangian formulation using appropriate *pull-back* operations. The resultant governing quantities are

$$\mathbf{P} = J\boldsymbol{\sigma}\mathbf{F}^{-\mathrm{T}}, \quad \mathbf{E} = \mathbf{F}^{\mathrm{T}}\mathbf{e}, \quad \mathbf{D} = J\mathbf{F}^{-1}\mathbf{d}, \tag{5}$$

referred to as the total first Piola–Kirchhoff stress, the Lagrangian electrical field and electric displacement fields, respectively. In terms of these quantities, the counterparts of equations (1) and (2) are

$$\nabla \cdot \mathbf{D} = 0, \quad \nabla \times \mathbf{E} = \mathbf{0}, \quad \nabla \cdot \mathbf{P} = \rho_0\mathbf{a}, \tag{6}$$

where $\rho_0 = J\rho$ is the mass density in the reference configuration. The jump conditions across the referential boundary are

$$\begin{aligned}(\mathbf{P} - \mathbf{P}^\star)\mathbf{N} = \mathbf{t}_M, \quad (\mathbf{E} - \mathbf{E}^\star) \times \mathbf{N} = \mathbf{0},\\ (\mathbf{D} - \mathbf{D}^\star) \cdot \mathbf{N} = -\omega_E,\end{aligned} \tag{7}$$

where $\mathbf{t}_M\mathrm{d}A = \mathbf{t}_m\mathrm{d}a$, $\omega_E\mathrm{d}A = \omega_e\mathrm{d}a$, and $\mathbf{N}$ is the outward unit normal vector of an element in the reference configuration.

Following Dorfmann and Ogden (2005), $\mathbf{P}$ and $\mathbf{E}$ in an incompressible material are derived from an augmented energy density function $\Psi(\mathbf{F}, \mathbf{D})$, via

$$\mathbf{P} = \frac{\partial\Psi}{\partial\mathbf{F}} - p_0\mathbf{F}^{-\mathrm{T}}, \quad \mathbf{E} = \frac{\partial\Psi}{\partial\mathbf{D}}; \tag{8}$$

the *Lagrange multiplier* p_0 accounts for the incompressibility constraint, and can be determined only in conjunction with the boundary conditions.

3. Acoustic waves in an array of soft dielectric tubes

In this section, we first detail the finite deformation that a single tube undergoes when subjected to a radial electric field under different mechanical constraints. The equations governing the propagation of sound through an infinite array of these tubes are provided next, together with a standard numerical method to solve them.

3.1. A soft dielectric tube in a radial electric field

The response of a soft dielectric tube subjected to a radial electric field has been reported in several instances (Singh 1966, Zhu *et al* 2010, Zhou *et al* 2014a, Shmuel 2015); herein, we apply the derivation in Shmuel and deBotton (2013) to a tube made of an elastomer exhibiting strain-stiffening at large deformations.

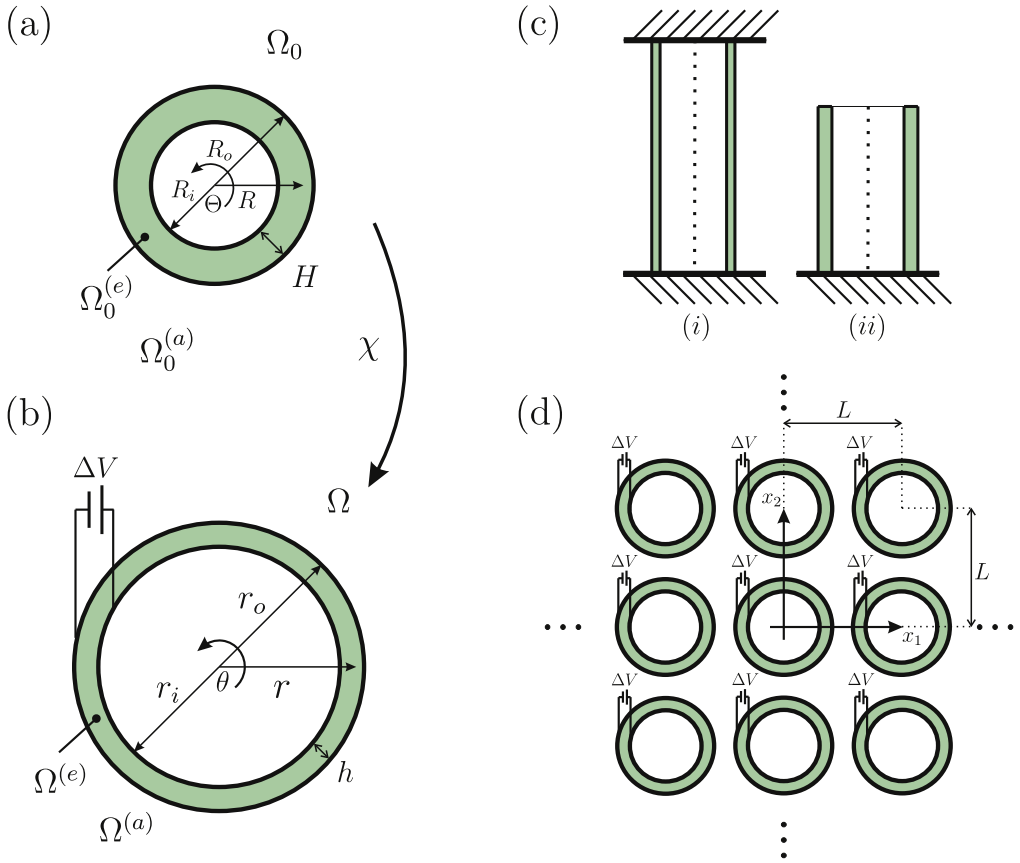

Figure 1. Dielectric elastomer tube in (a) the undeformed configuration, and (b) the deformed configuration, when subjected to a radial voltage difference. (c) Axial boundary conditions for the dielectric tube, namely, (i) axially clamped and (ii) axially free. (d) In-plane cross section of an infinite array of actuated soft dielectric tubes surrounded by air.

Accordingly, we consider an infinitely long tube made of an incompressible dielectric elastomer. The tube initial inner and outer radii are R_i and R_o, respectively, such that the reference thickness is $H = R_\mathrm{o} - R_\mathrm{i}$ (figure 1(a)). The tube occupies the region $\Omega_0^{(\mathrm{e})}$, and the remaining part of the domain, $\Omega_0^{(\mathrm{a})}$, is filled with air. Here and after, superscripts (e) and (a) denote quantities related to the elastomeric tube and to the air, respectively. The tube is subjected to a radial electric field by an application of a voltage ΔV between compliant electrodes coating its internal and external surfaces (figure 1(b)). The resultant deformation is described by the mapping

$$r = \sqrt{AR^2 + B}\,,\ \ \theta = \Theta,\ \ z = \frac{Z}{A}, \tag{9}$$

where (R, Θ, Z) and (r, θ, z) are the referential and the current cylindrical coordinates, respectively. The constants A and B depend on the boundary conditions. With respect to the above coordinate systems, the deformation gradient admits the following diagonal matrix representation

$$\mathsf{F} = \mathrm{diag}[\lambda_r, \lambda_\theta, \lambda_z], \tag{10}$$

where

$$\lambda_r = \frac{AR}{\sqrt{AR^2 + B}},\ \ \lambda_\theta = \frac{\sqrt{AR^2 + B}}{R},\ \ \lambda_z = \frac{1}{A}. \tag{11}$$

In terms of q_i—the charge per unit length accumulating on the interior electrode—the electric displacement field in the current configuration is

$$\mathbf{d} = d_r\hat{\mathbf{r}} = \frac{q_\mathrm{i}}{2\pi r}\hat{\mathbf{r}}. \tag{12}$$

To relate the deformation and the electrical variables, the constitutive behavior of the tube is to be specified. To this end, we make use of the widely accepted Gent energy function (Gent 1996, Zhou *et al* 2014b)

$$\Psi(\mathbf{F}, \mathbf{D}) = -\frac{\mu J_m}{2}\ln\left[1 - \frac{\mathrm{tr}(\mathbf{F}^\mathrm{T}\mathbf{F}) - 3}{J_m}\right] + \frac{1}{2\epsilon}\mathbf{D}\cdot\mathbf{F}^\mathrm{T}\mathbf{F}\mathbf{D}. \tag{13}$$

The constants ϵ and μ in the model conform respectively to the permittivity and the shear modulus of the material in the limit of small strains. The dimensionless parameter J_m models the strain-stiffening exhibited in elastomers, due to the finite extensibility of their polymer chains; in the limit $J_m \to \infty$, the neo-Hookean energy is recovered. The total stress resulting from equation (13) reads

$$\boldsymbol{\sigma} = \frac{\mu}{1 - \frac{\mathrm{tr}(\mathbf{F}^\mathrm{T}\mathbf{F}) - 3}{J_m}}\mathbf{b} + \frac{1}{\epsilon}\mathbf{d}\otimes\mathbf{d} - p_0\mathbf{I}. \tag{14}$$

Note that in equation (14) the multiplier of $\mathbf{b}$ reduces to μ when $J_m \to \infty$.

The equilibrium equations along direction θ and z show that the Lagrange multiplier p_0 is independent of these coordinates. The solution of the equilibrium equation along r

$$\sigma_{rr,r} + \frac{1}{r}(\sigma_{rr} - \sigma_{\theta\theta}) = 0, \tag{15}$$

reveals that p_0 is

$$\begin{aligned} p_0(r) = AB\mu\Bigg\{ & \frac{A^2 J_m[-B(A^3+C) + r^2(2A^3+C)]}{(2A^3+C)[A^3B^2 + (2A^3+C)r^2(r^2-B)]} \\ & - \frac{J_m}{AB}\ln r + \frac{J_m}{4AB\sqrt{2A^3+C}\sqrt{2A^3-C}} \\ & \times [(\mathrm{i}(2A^3-C) + \sqrt{2A^3+C}\sqrt{2A^3-C}) \\ & \times \ln(\mathrm{i}B\sqrt{2A^3-C} + (2r^2-B)\sqrt{2A^3+C}) \\ & + (-\mathrm{i}(2A^3-C) + \sqrt{2A^3+C}\sqrt{2A^3-C}) \\ & \times \ln(-\mathrm{i}B\sqrt{2A^3-C} + (2r^2-B)\sqrt{2A^3+C})] \\ & + \frac{q_i^2}{8\pi^2\epsilon\mu ABr^2}\Bigg\} + P, \end{aligned} \tag{16}$$

where $C = 1 - A^2(3 + J_m)$, and P is an integration constant. To complete the solution, boundary conditions are to be accounted. Firstly, we consider a cylindrical Gaussian surface outside the tube. Recalling that the problem exhibits an axial symmetry, it follows that there are no electric fields outside the tube, and therefore $\boldsymbol{\sigma}^\star = \mathbf{0}$. Since there are no mechanical tractions on the circumferential surfaces either, the radial boundary conditions are

$$\sigma_{rr}(r_\mathrm{i}) = 0, \quad \sigma_{rr}(r_\mathrm{o}) = 0, \tag{17}$$

where $r_\mathrm{i} \equiv r(R_\mathrm{i})$ and $r_\mathrm{o} \equiv r(R_\mathrm{o})$. Axially, we distinguish between the following two different conditions (figure 1(c)). (i) The tube is axially stretched and clamped at a fixed stretch ratio λ_z. In this case, the axial stretch λ_z is fixed, and thus the parameter A is a prescribed constant. Hence, the two radial conditions in equation (17) are sufficient to determine B. (ii) The tube is free to deform in the axial direction. Accordingly, A is unknown, and an additional boundary condition is required. As the top and bottom bases of the tube are free of mechanical loadings, the resultant axial force must vanish, and therefore

$$\int_0^{2\pi}\int_{r_\mathrm{i}}^{r_\mathrm{o}} \sigma_{zz} r \,\mathrm{d}r\mathrm{d}\theta = 0. \tag{18}$$

Allowing the tube to deform in the axial direction provides more than a variability of its length with the applied voltage—it enables a sharp *snap-through* transition between two deformation states of significantly different radii (Zhou *et al* 2014a, Cohen 2016). In section 4 to follow, we expand our discussion on this phenomenon, in relevance to our study.

Since in practice the controlled parameter is the voltage, we provide the connection between the surface charge and the applied voltage. The constitutive relation considered for the tube states that the relation between $\mathbf{e}$ and $\mathbf{d}$ is

$$\mathbf{e} = \frac{1}{\epsilon}\mathbf{d}; \tag{19}$$

accordingly, through equation (19) we relate the electric field and the charge via $e_r = q_\mathrm{i}/(\epsilon 2\pi r)$. The integration of the electric field along the radius provides

$$\Delta V = -\int_{r_\mathrm{i}}^{r_\mathrm{o}} e_r \mathrm{d}r = \frac{q_\mathrm{i}}{2\pi\epsilon}\ln\left(\frac{r_\mathrm{o}}{r_\mathrm{i}}\right). \tag{20}$$

3.2. Acoustic wave propagation in an array of deformable dielectric tubes

Consider next an infinite array of tubes in a periodic square arrangement, such that the center-to-center distance of adjacent tubes is L (figure 1(d)). Each tube is deformed by the application of voltage, as described in section 3.1. We examine acoustic waves propagating through the periodicity plane of the deformed array. Note that each tube in the assembly is activated independently. This offers, in principle, the possibility to modulate and deform particular tubes differently, thereby creating a tunable waveguide which confines and guides acoustic waves. This approach will be explored in future works; our current investigation considers the case in which all the tubes are subjected to the same voltage ΔV.

Strictly, the interaction of the acoustic waves with the solid should depend on the instantaneous moduli of the deformed tubes, and may result in sound penetration into the solid. However, the huge contrast between the impedance of the air and the solid practically causes total reflection of incident waves, confining them to the air. This justifies a simplified approach which considers the solid as rigid cylinders, resulting with a scalar equation for the acoustic pressure (Sigalas and Economou 1996a, Kafesaki and Economou 1999, Cervera *et al* 2002, Vasseur *et al* 2002, Maldovan and Thomas 2009). In accordance with the total reflection at the interface, there are no electric perturbations since the waves are confined to the air, where there are no electric fields. Therefore, acoustic wave propagation through the array is described by the equation

$$\nabla_\mathrm{T}\cdot\left(\frac{1}{\rho(\mathbf{x})}\nabla_\mathrm{T} p(\mathbf{x}, t)\right) = \frac{1}{K(\mathbf{x})}p_{,tt}(\mathbf{x}, t), \tag{21}$$

where $p(\mathbf{x}, t)$ is the acoustic pressure field, and $\nabla_\mathrm{T}(\bullet) = (\bullet)_{,1}\mathbf{i}_1 + (\bullet)_{,2}\mathbf{i}_2$ is the in-plane gradient operator, $\mathbf{i}_j$ denotes the unit vector in the x_j-direction. In a linear isotropic elastic medium, $K(\mathbf{x})$ is the bulk modulus. Indeed, based on the simplified approach, numerical solutions to equation (21) agree with experimental measurements (Cervera *et al* 2002, Pichard *et al* 2012, Babaee *et al* 2016, Jiang *et al* 2017). We note that, rigorously, the deformed tube is a transversely isotropic material whose properties vary along the radius. In the rigid cylinder approximation, however, to represent the corresponding perfectly reflecting boundary conditions at the outer boundary (Goffaux and Vigneron 2001, Babaee *et al* 2016), it is sufficient to consider a sufficiently large piecewise constant $K(\mathbf{x})$ at $\mathbf{x} \in \Omega^{(\mathrm{e})}$[1]. We further note that while equation (21) is purely

[1] This has been observed in a series of calculations we performed with different fields of $K(\mathbf{x})$. This is also in agreement with the calculations of Kafesaki and Economou (1999), who demonstrated that when the impedance contrast is huge, the exact stiffness of the scatterers does not affect the band structure.

mechanical, it is affected by the bias electric field, since that field determines the location of the air/solid interface. In other words, the voltage controls at which $\mathbf{x}$ the fields $\rho(\mathbf{x})$ and $K(\mathbf{x})$ correspond to the air.

Equation (21) is solved by means of the plane wave expansion method. The simplicity of the method has led to its popularity in calculating band diagrams in quantum mechanics and optics, and also in solid mechanics (Kushwaha *et al* 1993, 1998, Sigalas and Economou 1996b, Vasseur *et al* 2002, Barnwell *et al* 2016, 2017, Getz *et al* 2016). The method rests on the fact that plane waves constitute a basis for the solution of equation (21). Thus, the idea is to represent periodic fields in Fourier series to derive a computational eigenvalue problem. Accordingly, we first employ a Fourier representation of the functions $\rho^{-1}(\mathbf{x})$ and $K^{-1}(\mathbf{x})$, namely,

$$\zeta(\mathbf{x}) = \sum_{\mathbf{G}} \zeta(\mathbf{G}) \exp(\mathrm{i}\mathbf{G}\cdot\mathbf{x}), \qquad \zeta = \frac{1}{\rho}, \frac{1}{K}. \tag{22}$$

Herein, $\{\zeta(\mathbf{G})\}$ is the set of Fourier coefficients, defined by

$$\zeta(\mathbf{G}) = \frac{1}{L^2}\iint_{a_{\mathrm{cell}}} \zeta(\mathbf{x})\exp(-\mathrm{i}\mathbf{G}\cdot\mathbf{x})\mathrm{d}a, \tag{23}$$

where $\left\{\mathbf{G} = \frac{2\pi}{L} n_1\mathbf{i}_1 + \frac{2\pi}{L} n_2\mathbf{i}_2,\ n_1, n_2 \in \mathbb{N}\right\}$ is the set of reciprocal lattice vectors, and a_{cell} is the area of the unit cell in Ω.

Making use of the fact that $\zeta(\mathbf{x})$ is piecewise constant at $\mathbf{x} \in \Omega^{(\mathrm{a})}$ and $\mathbf{x} \in \Omega^{(\mathrm{e})}$, we rewrite $\zeta(\mathbf{G})$ in the form

$$\zeta(\mathbf{G}) = \begin{cases} v\zeta^{(\mathrm{e})} + (1-v)\zeta^{(\mathrm{a})} & \mathbf{G} = \mathbf{0}, \\ (\zeta^{(\mathrm{e})} - \zeta^{(\mathrm{a})})F(\mathbf{G}) & \mathbf{G} \neq \mathbf{0}, \end{cases} \tag{24}$$

where

$$F(\mathbf{G}) = \frac{1}{L^2}\iint_{a^{(\mathrm{e})}} \exp(-\mathrm{i}\mathbf{G}\cdot\mathbf{x})\mathrm{d}a = 2v\frac{J_1(Gr_{\mathrm{o}})}{Gr_{\mathrm{o}}}; \tag{25}$$

here, J_1 is the Bessel function of the first kind of order 1, $v = \pi r_{\mathrm{o}}^2/L^2$ and $a^{(\mathrm{e})}$ are the volume fraction and the area of a solid cylinder of radius $r = r_{\mathrm{o}}$ in Ω, respectively.

Subsequently, the acoustic pressure field $p(\mathbf{x}, t)$ is expressed in the Bloch form

$$p(\mathbf{x}, t) = \sum_{\mathbf{G}} p(\mathbf{G})\exp[\mathrm{i}(\mathbf{G}+\mathbf{k})\cdot\mathbf{x} - \mathrm{i}\omega t], \tag{26}$$

where the Bloch wave vector is $\mathbf{k} = k_1\mathbf{i}_1 + k_2\mathbf{i}_2$, $k_1, k_2 \in \mathbb{R}$, and ω is the angular frequency. Equation (26) is established by the Bloch theorem (Kittel 2005). In terms of equations (24) and (26), equation (21) becomes

$$\left\{\sum_{\mathbf{G}'}\left[\frac{1}{\rho}(\mathbf{G})p(\mathbf{G}')(\mathbf{G}'+\mathbf{k})\cdot(\mathbf{G}+\mathbf{G}'+\mathbf{k}) - \omega^2\frac{1}{K}(\mathbf{G})p(\mathbf{G}')\right]\exp[\mathrm{i}(\mathbf{G}+\mathbf{G}')\cdot\mathbf{x} - \mathrm{i}\omega t]\right\} \times \exp(\mathrm{i}\mathbf{k}\cdot\mathbf{x}) = 0. \tag{27}$$

Since equation (27) holds for any $\mathbf{x}$, the sum in the curly brackets must vanish. We multiply this sum by $\exp(-\mathrm{i}\,\mathbf{G}''\cdot\mathbf{x})$, and integrate the result over the unit-cell. Due to the orthogonality property of the Fourier series, the only non-vanishing terms are those satisfying the condition $\mathbf{G}'' = \mathbf{G} + \mathbf{G}'$. Thus, the resultant equation is

$$\sum_{\mathbf{G}'}\frac{1}{\rho}(\mathbf{G}-\mathbf{G}')p(\mathbf{G}')(\mathbf{G}'+\mathbf{k})\cdot(\mathbf{G}+\mathbf{k}) = \omega^2\sum_{\mathbf{G}'}\frac{1}{K}(\mathbf{G}-\mathbf{G}')p(\mathbf{G}'). \tag{28}$$

We write equation (28) in the following matrix form

$$\mathsf{Q}\mathsf{p} = \omega^2\mathsf{R}\mathsf{p}, \tag{29}$$

where Q and R are matrices whose components are

$$\mathsf{Q}_{\mathbf{G},\mathbf{G}'} = (\mathbf{G}'+\mathbf{k})\cdot(\mathbf{G}+\mathbf{k})\rho^{-1}(\mathbf{G}-\mathbf{G}'), \tag{30}$$

$$\mathsf{R}_{\mathbf{G},\mathbf{G}'} = K^{-1}(\mathbf{G}-\mathbf{G}'), \tag{31}$$

and p is a column vector containing the Fourier components $p(\mathbf{G}')$.

The band structure is constructed by solving numerically equation (29) for ω as a function of $\mathbf{k}$, using a finite truncation of the number of plane waves. We note that to calculate gaps in the diagram, it is sufficient in certain cases to consider only values of $\mathbf{k}$ at the edges of the irreducible first Brillouin zone (Harrison *et al* 2007, Craster *et al* 2012). These intervals connect the points $\Gamma = (0, 0)$, $X = (\pi/L, 0)$ and $M = (\pi/L, \pi/L)$. In our computational examples, a number of 169 plane waves, corresponding to $-6 \leqslant n_1, n_2 \leqslant 6$, was found sufficient for the convergence of the band structure.

4. Parametric study

Through numerical examples, we study how the mechanical constraints and the applied voltage affect the acoustic band gap in the audible frequency range 0–10 kHz. To this end, we consider exemplary tubes whose initial inner and outer radii are $R_{\mathrm{i}} = 10$ mm and $R_{\mathrm{o}} = 12.5$ mm, respectively. The mass density, shear modulus, locking parameter and dielectric constant of the elastomer are set to the representative values

$$\rho^{(\mathrm{e})} = 1000\ \mathrm{kg\ m^{-3}}, \quad \mu^{(\mathrm{e})} = 350\ \mathrm{kPa}, \quad J_m^{(\mathrm{e})} = 10, \quad \varepsilon^{(\mathrm{e})} = 3\varepsilon_0. \tag{32}$$

In the modeling of the tubes as rigid scatterers, we set the constant $K^{(\mathrm{e})}$ to 10^7 kPa[2]. The *dielectric strength* of the elastomer—the maximum electric field that a dielectric can withstand without loosing its insulating property—is set to 100 MV m^{-1}. The density and the bulk modulus of the air are set to the characteristic values

$$\rho^{(\mathrm{a})} = 1.2\ \mathrm{kg\ m^{-3}}, \quad K^{(\mathrm{a})} = 141\ \mathrm{kPa}. \tag{33}$$

[2] As mentioned earlier, additional calculations using varying and larger values of $K^{(\mathrm{e})}$ yielded the same results.

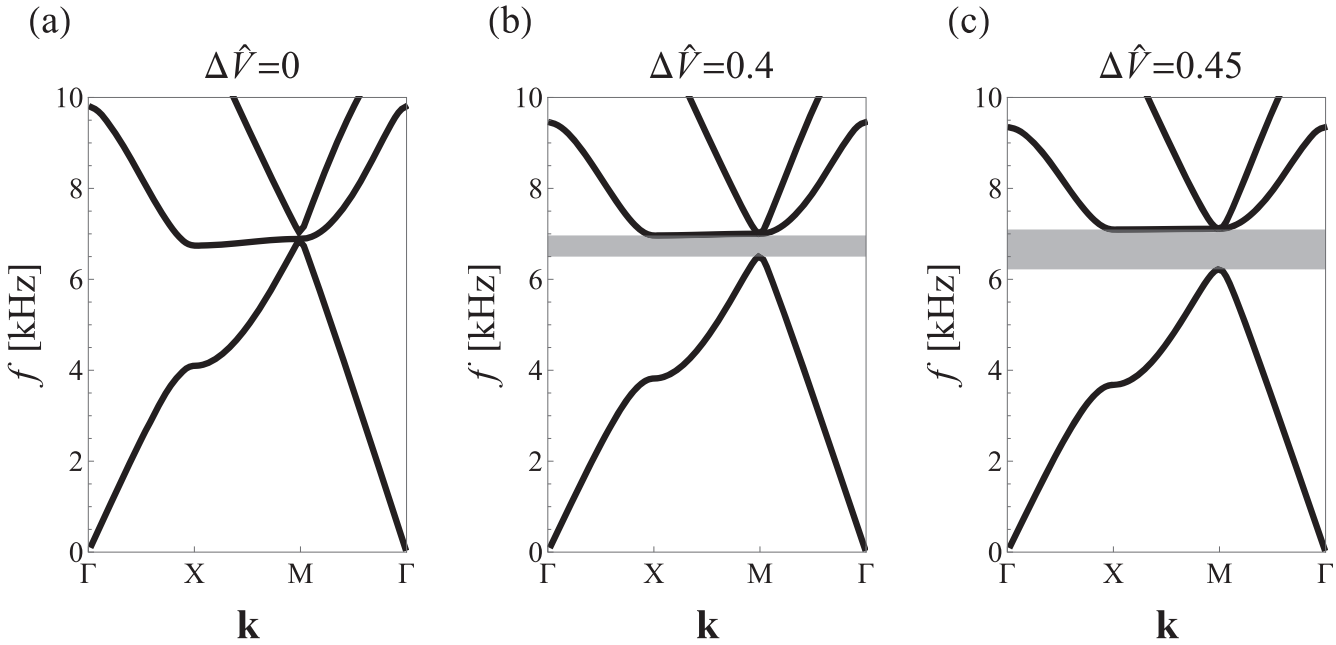

Figure 2. Band diagram of a square array of pre-stretched tubes, clamped at $\lambda_z = 2$, whose center-to-center distance is $L = 30$ mm, and subjected to the normalized voltages (a) $\Delta\hat{V} = 0$, (b) $\Delta\hat{V} = 0.4$ and (c) $\Delta\hat{V} = 0.45$.

We examine first tubes with clamped top and bottom surfaces, whose center-to-center spacing is 30 mm, such that the distance between adjacent tube surfaces at the most deformed examined configuration is $H/2$. We evaluate the band diagram in terms of the ordinary frequency $f = \omega/2\pi$, for increasing values of an applied normalized voltage $\Delta\hat{V} = \Delta V/H\sqrt{\varepsilon/\mu}$, up to the onset of electric breakdown. Accordingly, figure 2 shows the band diagram of pre-stretched tubes clamped at $\lambda_z = 2$, and subjected to exemplary normalized voltages $\Delta\hat{V} = 0$ (figure 2(a)), $\Delta\hat{V} = 0.4$ (figure 2(b)) and $\Delta\hat{V} = 0.45$ (figure 2(c)). We observe that without the application of voltage there is no *complete* gap in the diagram, i.e., a gap in all directions defined by $\mathbf{k}$; by contrast, a directional gap is observed, e.g., along *XM* across the frequencies $0 - 4$ kHz. In what follows, we focus on the existence of complete gaps. With the application of a sufficiently high voltage a complete gap opens, designated by the gray region in the diagram, such that at $\Delta\hat{V} = 0.4$ its width is $\simeq$0.5 kHz, and at $\Delta\hat{V} = 0.45$ its width is $\simeq$0.8 kHz.

By extracting gap widths from successive band diagrams, we evaluate in figures 3(a)–(c) the acoustic band gap when the tubes are clamped at their initial axial length ($\lambda_z = 1$), and stretched and clamped at $\lambda_z = 1.5$ and $\lambda_z = 2$, respectively, as a function of the normalized voltage $\Delta\hat{V}$. Note that the maximal voltage applied at each stretch is the critical value which triggers electric breakdown; this value becomes lower when the tube is stretched, due to the corresponding reduction in thickness and subsequent increase in the electric field.

As observed in figure 2, when the tubes are clamped at their initial axial length, the central frequency of the band gap is 6.5 kHz; as the voltage is increased, the gap width increases from 2.09 to 5.26 kHz, and the central frequency is slightly lowered. The relative change between gap widths at high values of voltage is significantly more evident. For instance, the relative change in the gap width is 45% between $\Delta\hat{V} = 0.6$ and 0.7, while it is only 1.2% between $\Delta\hat{V} = 0$ and 0.1. We also evaluate the gap as predicted by a neo-Hookean model, and indicate its edges with dashed curves; the difference between the prediction of the two elasticity models is almost indistinguishable. The reason is that the corresponding strains are not significant enough to trigger the lock-up phenomenon, which differentiates the Gent model from the neo-Hookean model.

When the tubes are stretched and clamped at $\lambda_z = 1.5$, the central frequency of the band gap is 6.7 kHz; as the voltage is increased, the gap width increases from 0.44 to 1.88 kHz, and the central frequency is slightly lowered. Again, the relative change in the gap width between high values of voltage is more drastic; the relative change in the gap width is 69% between $\Delta\hat{V} = 0.43$ and 0.53, where it is 5.3% between between $\Delta\hat{V} = 0$ and 0.1. These results are almost the same for the neo-Hookean model.

When the tubes are stretched and clamped at $\lambda_z = 2$, there is no gap without the application of voltage, since the resultant cylinders are too small to create sufficient scattering and interference. With the application of a normalized voltage of $\Delta\hat{V} \simeq 0.35$, the cylinders reach a threshold radius at which a gap opens with a central frequency of 6.8 kHz; for the neo-Hookean model, this cut-off voltage is $\Delta\hat{V} \simeq 0.25$. Note that in this case the two elasticity models hence provide different predictions; the predicted breakdown voltage and the acoustic gap are also different. Particularly, the maximal width of the gap is 0.88 kHz according to the Gent model, and 1.32 kHz according to the neo-Hookean model.

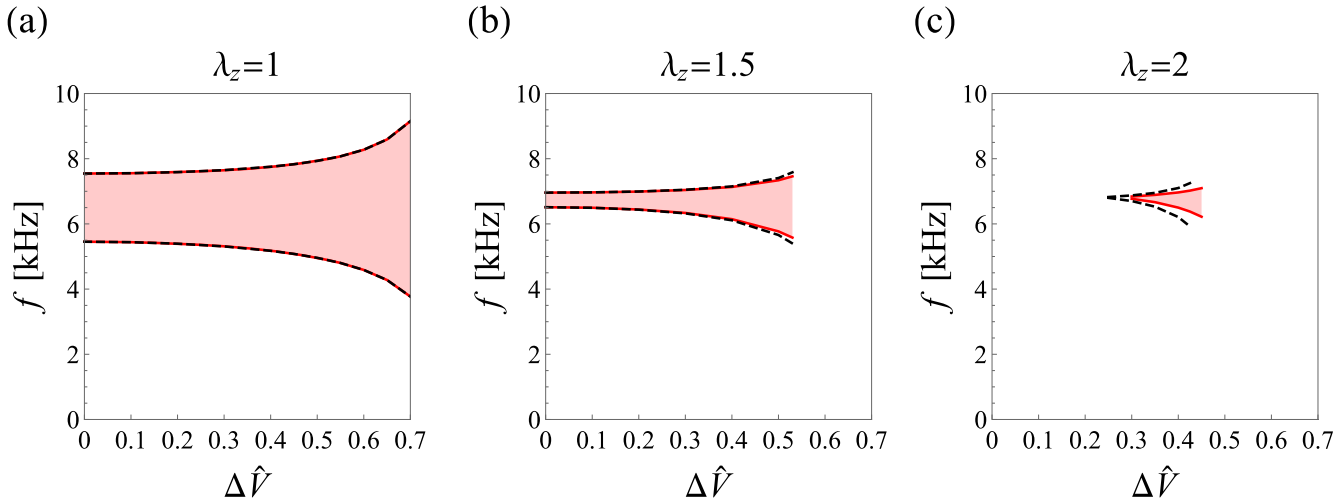

Figure 3. Acoustic band gap as a function of the normalized applied voltage $\Delta\hat{V}$, for a square array of a lattice parameter $L = 30$ mm. The tubes are (a) clamped at their initial length $\lambda_z = 1$, and stretched and clamped at (b) $\lambda_z = 1.5$ and (c) $\lambda_z = 2$. Continuous and dashed lines correspond to the band gap boundaries as predicted by the Gentian and the neo-Hookean models, respectively.

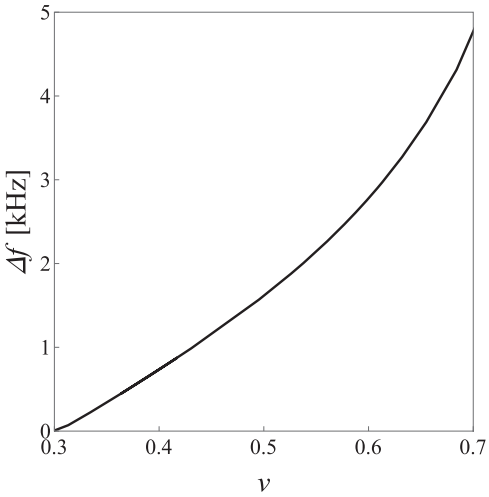

Figure 4. Gap width as a function of the volume fraction v enclosed by the deformed tubes external radius r_o, in a square array of a lattice parameter $L = 30$ mm.

Comparison of the different cases in figure 3 shows that axially stretching the tubes shifts the central frequency of the gap towards a slightly higher frequency. More importantly, it is evident that an increase in the axial stretch of the tube narrows the gap, while an increase in the applied voltage widens it. Thus, the mechanical stretch and applied voltage offer, in principle, complementary mechanisms to control the width and the location of the acoustic gap. Recalling that the enclosed volume is reduced when the tubes are stretched, and is increased when voltage is applied, the exhibited trends agree with the relation between the gap and the volume fraction shown by Kushwaha (1997).

We calculate the volume enclosed within the deformed external radius r_o at each applied voltage from the three cases in figure 3, to evaluate in figure 4 the gap width as function the corresponding volume fraction v. We observe that identical volume fractions at different loading conditions yield the same gap width. We further observe that a threshold volume fraction is required to open the gap. Beyond that threshold, the gap width increases monotonically with this volume fraction. These results are in agreement with the findings of Kushwaha (1997) and Sánchez-Pérez *et al* (1998).

We examine next the arrangement in which the tubes are free to extend. Before we explore the dependency of the acoustic gap on the voltage, we momentarily dwell on the underlaying static deformation. Specifically, we present in figure 5(a) the relation between the outer radius of the axially free tubes, and the applied voltage. The Gent model, denoted by the continuous curve, predicts that two solutions, indicated by points B and B', exist for $\Delta\hat{V} \simeq 0.7$. Since the deformation path along the convex curve between the states is unstable, the tubes may suddenly snap from state B to B', thereby undergoing a drastic change in their outer radius (Zhou *et al* 2014a); this path is indicated by a right arrow in figure 5(a). The neo-Hookean model, denoted by the dashed curve, does not capture this transition. We explain next the reason for this sudden transition, and why the Gent model can predict it, whereas the neo-Hookean cannot. To this end, we first recall that the evolving stress consists of an elastic response which equilibrates a compressive stress due to the electric load. The stress state is accompanied by a reduction in thickness and enlargement of the radii. Beyond a threshold voltage, the electrostatic part of the stress can be accommodated only through a drastic rise in the mechanical stress. This is achieved when the tube stiffens through the stretching of the comprising polymer chains towards their limiting strain. Macroscopically, this process corresponds to a snap-through transition between two significantly different configurations of the tube. Since the Gent model was develop to capture the stiffening of the elastomer at high strains, it indeed predicts the snapping of tube. The neo-Hookean model is unable to model the rapid elastomeric

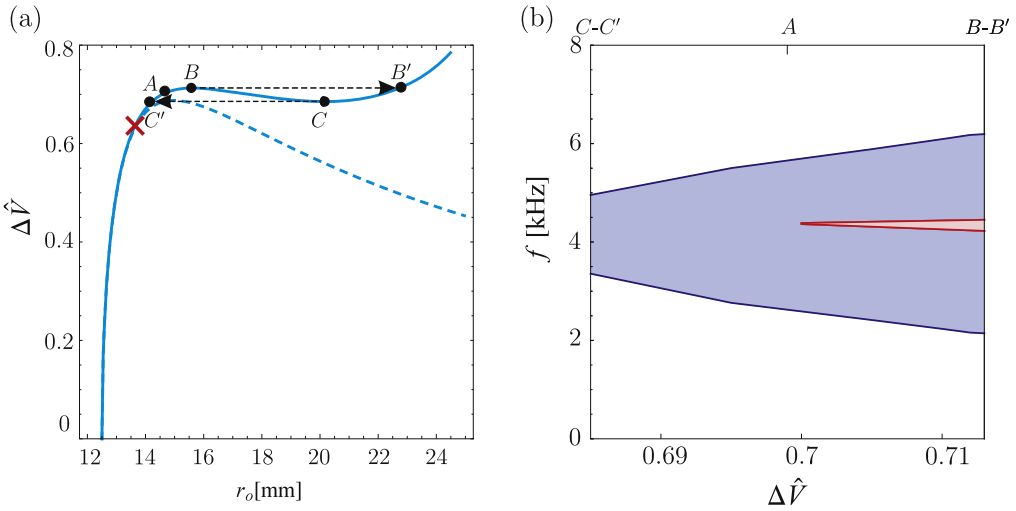

Figure 5. (a) Normalized voltage versus deformed outer radius r_o for an axially free tube. The red cross denotes the onset of electric breakdown. Dashed arrows indicate snap-through transitions. Continuous and dashed lines denote the Gent and the neo-Hookean models, respectively. (b) Acoustic band gap as a function of the normalized applied voltage $\Delta\hat{V}$ for a square array of axially free tubes, characterized by lattice parameter $L = 46.7$ mm. Red and blue regions denote the gap before and after the snap-through, respectively.

stiffening, and therefore it predicts that there are no possible equilibria beyond a critical voltage. For a further discussion on this phenomenon and the difference between the models, the reader is referred to, e.g., Li *et al* (2011) and Cohen (2016). A snap-through triggered by voltage has been experimentally observed and exploited before to achieve a transition between significantly different deformations (Keplinger *et al* 2012, Li *et al* 2013). In what follows, we demonstrate how this phenomenon can be potentially harnessed to open and tune the acoustic gap. We note that the dielectric strength of standard elastomers hinders the realization of such a transition, as it occurs beyond their typical point of electric breakdown (marked with a red cross in figure 5(a)). However, we believe that ongoing works on the enhancement of the dielectric strength of elastomers through changes in their synthesization will render our theoretical predictions realizable (Madsen *et al* 2014, 2015).

We thus evaluate in figure 5(b) the acoustic gap of an array of axially free tubes, as function of the normalized voltage; we now consider a center-to-center spacing of 46.7 mm, to accommodate the snap-through transition. A gap with the central frequency 4.3 kHz opens at $\Delta\hat{V} = 0.7$ (state A in figure 5(a)), and reaches a width of $\sim$0.23 kHz near the verge of snapping at $\Delta\hat{V} = 0.713$; this gap is indicated in figure 5(b) by the red region. When snapping is triggered and the tubes transition from state B to state B', the gap width drastically changes to 4.048 kHz. A subsequent decrease in voltage to $\Delta\hat{V} \simeq 0.685$ narrows the gap, as indicated by the blue region in figure 5(b). A further incremental decrease in voltage triggers a contracting snap-through transition from state C to state C', as indicated by the left arrow in figure 5(a), and the closure of the gap. In principle, these states and their corresponding gap width can be reached repeatedly by a cyclic application of voltage.

5. Conclusions

We have theoretically demonstrated a new approach to tune acoustic band gaps across audible frequencies, using an array of elastomeric tubes. Our approach utilizes configurations the tubes are brought about when radial voltage is applied, to manipulate sound propagation via the deformed array. The electrostatic deformation has been determined using an exact analytic solution based on nonlinear electroelasticity; the propagation of acoustic waves through the actuated tubes has been calculated using the plane wave expansion method.

Using a parametric study of the band diagram corresponding to the deformed array, we have studied how the mechanical boundary conditions and the applied voltage change the acoustic characteristics. We have used representative values of the physical properties of dielectric elastomers to model the tubes. Our first investigation considered an array whose comprising tubes are stretched and then axially clamped, such that their length is fixed. Our calculations have shown that axially stretching the tubes narrows the acoustic gap. Conversely, the gap is rendered wider by the application of voltage. Our second investigation considered an array whose comprising tubes are free to elongate in the axial direction. Here again, the width of the gap is enlarged with higher values of voltage. Interestingly, the gap changes abruptly at two particular values of voltage, in contrast with the continuous change of the gap when the tubes are clamped. These values of voltage trigger a snap-through transition between extremely different states of deformation, and hence induce a drastic change in the gap width. Thereby, we have demonstrated that snap-through instabilities resulting from geometrical and material nonlinearities can be harnessed to achieve sharp transitions in the acoustic gap. Our envisioned system thus offers a new way to tune sonic band gaps, using a simple adjustment of applied voltage.

Acknowledgments

The authors acknowledge the support of the Israel Science Foundation, founded by the Israel Academy of Sciences and Humanities (Grant No. 1912/15). EB also thanks the Technion fellowship by Lady Davis Foundation.

References

Babaee S, Viard N, Wang P, Fang N X and Bertoldi K 2016 Harnessing deformation to switch on and off the propagation of sound *Adv. Mater.* **8** 1631–5

Barnwell E G, Parnell W J and Abrahams I D 2017 Tunable elastodynamic band gaps *Extreme Mech. Lett,* **12** 23–9

Barnwell E G, Parnell W J and Abrahams I D 2016 Antiplane elastic wave propagation in pre-stressed periodic structures; tuning, band gap switching and invariance *Wave Motion* **63** 98–110

Brochu P and Pei Q 2010 Advances in dielectric elastomers for actuators and artificial muscles *Macromol. Rapid Commun.* **31** 10–36

Castañeda P P and Siboni M H 2012 A finite-strain constitutive theory for electro-active polymer composites via homogenization *Int. J. Non-Linear. Mech.* **47** 293–306

Cervera F, Sanchis L, Sánchez-Pérez J V, Martínez-Sala R, Rubio C, Meseguer F, López C, Caballero D and Sánchez-Dehesa J 2002 Refractive acoustic devices for airborne sound *Phys. Rev. Lett.* **88** 239021

Cohen N 2017 Stacked dielectric tubes with electromechanically controlled radii *Int. J. Solids Struct.* **108** 40–8

Craster R V, Antonakakis T, Makwana M and Guenneau S 2012 Dangers of using the edges of the brillouin zone *Phys. Rev.* B **86** 115130

Dorfmann A and Ogden R W 2005 Nonlinear electroelasticity *Acta. Mech.* **174** 167–83

Frazier M J and Kochmann D M 2017 Band gap transmission in periodic bistable mechanical systems *J. Sound Vib.* **388** 315–26

Gei M, Roccabianca S and Bacca M 2011 Controlling bandgap in electroactive polymer-based structures *IEEE/ASME Trans. Mechatronics* **16** 102–7

Gent A N 1996 A new constitutive relation for rubber *Rubber Chem. Technol.* **69** 59–61

Getz R, Kochmann D M and Shmuel G 2016 Voltage-controlled complete stopbands in two-dimensional soft dielectrics *Int. J. Solids Struct.* doi:10.1016/j.ijsolstr.2016.10.002

Goffaux C and Vigneron J P 2001 Theoretical study of a tunable phononic band gap system *Phys. Rev.* B **64** 075118

Gorishnyy T, Maldovan M, Ullal C and Thomas E 2005 Sound ideas *Phys. World* **18** 24

Harrison J M, Kuchment P, Sobolev A and Winn B 2007 On occurrence of spectral edges for periodic operators inside the brillouin zone *J. Phys. A: Math. Theor.* **40** 7597

Hussein M I, Leamy M J and Ruzzene M 2014 Dynamics of phononic materials and structures: historical origins, recent progress, and future outlook *Appl. Mech. Rev.* **66** 040802

Jia K, Wang M, Lu T, Zhang J and Wang T 2016 Band-gap tunable dielectric elastomer filter for low frequency noise *Smart Mater. Struct.* **25** 055047

Jiang G, Liu Y, Wu Y, Xu W, Kong Q and Zhang C 2017 Transmission and radiation of acoustic oblique incident through tube arrays based on phononic crystals theory *Appl. Acoust.* **116** 117–26

Kafesaki M and Economou E N 1999 Multiple-scattering theory for three-dimensional periodic acoustic composites *Phys. Rev.* B **60** 11993–2001

Keplinger C, Li T, Baumgartner R, Suo Z and Bauer S 2012 Harnessing snap-through instability in soft dielectrics to achieve giant voltage-triggered deformation *Soft Matter* **8** 285–8

Kittel C 2005 *Introduction to Solid State Physics* (Hoboken, NJ: Wiley)

Kushwaha M S 1997 Stop-bands for periodic metallic rods: Sculptures that can filter the noise *Appl. Phys. Lett.* **70** 3218–20

Kushwaha M S, Djafari-Rouhani B, Dobrzynski L and Vasseur J O 1998 Sonic stop-bands for cubic arrays of rigid inclusions in air *Eur. Phys. J.* B **3** 155–61

Kushwaha M S, Halevi P, Dobrzynski L and Djafari-Rouhani B 1993 Acoustic band structure of periodic elastic composites *Phys. Rev. Lett.* **71** 2022–5

Li B, Chen H, Qiang J, Hu S, Zhu Z and Wang Y 2011 Effect of mechanical pre-stretch on the stabilization of dielectric elastomer actuation *J. Phys. D: Appl. Phys.* **44** 155301

Li T, Keplinger C, Baumgartner R, Bauer S, Yang W and Suo Z 2013 Giant voltage-induced deformation in dielectric elastomers near the verge of snap-through instability *J. Mech. Phys. Solids* **61** 611–28

Liu Y, Liu L, Zhang Z and Leng J 2009 Dielectric elastomer film actuators: characterization, experiment and analysis *Smart Mater. Struct.* **18** 095024

Lopez-Pamies O 2014 Elastic dielectric composites: theory and application to particle-filled ideal dielectrics *J. Mech. Phys. Solids* **64** 61–82

Madsen F B, Yu L, Daugaard A E, Hvilsted S and Skov A L 2014 Silicone elastomers with high dielectric permittivity and high dielectric breakdown strength based on dipolar copolymers *Polymer* **55** 6212–9

Madsen F B, Yu L, Daugaard A E, Hvilsted S and Skov A L 2015 A new soft dielectric silicone elastomer matrix with high mechanical integrity and low losses *RSC Adv.* **5** 10254–9

Maldovan M and Thomas E L 2009 Phononic crystals *Periodic Materials and Interference Lithography* (Weinheim: Wiley) pp 183–213

Overvelde J T B, Kloek T, D'haen J J A and Bertoldi K 2015 Amplifying the response of soft actuators by harnessing snap-through instabilities *Proc. Natl Acad. Sci. USA* **112** 10863–8

Pelrine R, Kornbluh R, Pei Q-B and Joseph J 2000 High-speed electrically actuated elastomers with strain greater than 100% *Science* **287** 836–9

Pichard H, Richoux O and Groby J-P 2012 Experimental demonstrations in audible frequency range of band gap tunability and negative refraction in two-dimensional sonic crystal *J. Acoust. Soc. Am.* **132** 2816–22

Picó R, Pérez-Arjona I, Sánchez-Morcillo V J and Staliunas K 2013 Evidences of spatial (angular) filtering of sound beams by sonic crystals *Appl. Acoust.* **74** 945–8

Raney J, Nadkarni N, Daraio C, Kochmann D M, Lewis J A and Bertoldi K 2016 Stable propagation of mechanical signals in soft media using stored elastic energy *Proc. Natl Acad. Sci. USA* **113** 9722–27

Robillard J-F, Matar O B, Vasseur J O, Deymier P A, Stippinger M, Hladky-Hennion A-C, Pennec Y and Djafari-Rouhani B 2009 Tunable magnetoelastic phononic crystals *Appl. Phys. Lett.* **95** 124104

Sánchez-Pérez J V, Caballero D, Martínez-Sala R, Rubio C, Sánchez-Dehesa J, Meseguer F, Llinares J and Galvez F 1998 Sound attenuation by a two-dimensional array of rigid cylinders *Phys. Rev. Lett.* **80** 5325–8

Schlaak H F, Gei M, Bortot E, Haus H and Mößinger H 2016 *Dielectric Elastomers as EAPs: Models* (Springer International Publishing) pp 1–24

Shim J, Wang P and Bertoldi K 2015 Harnessing instability-induced pattern transformation to design tunable phononic crystals *Int. J. Solids Struct.* **58** 52–61

Shmuel G 2015 Manipulating torsional motions of soft dielectric tubes *J. Appl. Phys.* **117** 174902

Shmuel G and deBotton G 2013 Axisymmetric wave propagation in finitely deformed dielectric elastomer tubes *Proc. R. Soc.* A **469** 20130071

Shmuel G and Pernas-Salomón R 2016 Manipulating motions of elastomer films by electrostatically-controlled aperiodicity *Smart Mater. Struct.* **25** 125012

Sigalas M M and Economou E N 1992 Elastic and acoustic wave band structure *J. Sound Vib.* **158** 377–82

Sigalas M M and Economou E N 1996a Attenuation of multiple-scattered sound *Europhys. Lett.* **36** 241–6

Sigalas M M and Economou E N 1996b Attenuation of multiple scattered sound *Europhys. Lett.* **36** 241

Singh M and Pipkin A C 1966 Controllable states of elastic dielectrics *Arch. Ration. Mech. Anal.* **21** 169–210

Suo Z, Zhao X and Greene W H 2008 A nonlinear field theory of deformable dielectrics *J. Mech. Phys. Solids* **56** 467–86

Vasseur J O, Deymier P A, Djafari-Rouhani B, Pennec Y and Hladky-Hennion A-C 2008 Absolute forbidden bands and waveguiding in two-dimensional phononic crystal plates *Phys. Rev.* B **77** 085415

Vasseur J O, Deymier P A, Khelif A, Lambin P, Djafari-Rouhani B, Akjouj A, Dobrzynski L, Fettouhi N and Zemmouri J 2002 Phononic crystal with low filling fraction and absolute acoustic band gap in the audible frequency range: a theoretical and experimental study *Phys. Rev.* E **65** 056608

Wang L and Bertoldi K 2012 Mechanically tunable phononic band gaps in three-dimensional periodic elastomeric structures *Int. J. Solids Struct.* **49** 2881–5

Wu B, Su Y, Chen W and Zhang C 2017 On guided circumferential waves in soft electroactive tubes under radially inhomogeneous biasing fields *J. Mech. Phys. Solids* **99** 116–45

Yang W P and Chen L W 2008 The tunable acoustic band gaps of two-dimensional phononic crystals with a dielectric elastomer cylindrical actuator *Smart Mater. Struct.* **17** 015011

Yu X, Lu Z, Cui F, Cheng L and Cui Y 2017 Tunable acoustic metamaterial with an array of resonators actuated by dielectric elastomer *Extreme Mech. Lett.* **12** 37–40

Zhou J, Jiang L and Khayat R E 2014a Electromechanical response and failure modes of a dielectric elastomer tube actuator with boundary constraints *Smart Mater. Struct.* **23** 045028

Zhou J, Jiang L and Khayat R E 2014b Electromechanical response and failure modes of a dielectric elastomer tube actuator with boundary constraints *Smart Mater. Struct.* **23** 045028

Zhu J, Stoyanov H, Kofod G and Suo Z 2010 Large deformation and electromechanical instability of a dielectric elastomer tube actuator *J. Appl. Phys.* **108** 074113